CFD-Based Aerothermal Design Verification of Coffee Cabinet Dryer

Gerry M. Castillo[1], Aeron R. Mojica[2], Jhon Heron P. Carsocho[3],
Ray Rojan C. Romeroso[4], Sheryl Dinglasan-Fenol[5], Al Eugene L. Torres[6], Gee Jay C. Bartolome[7]
College of Engineering and Information Technology, Cavite State University, Indang, Cavite, Philippines[1]
National Coffee Research, Development and Extension Center, Cavite State University, Indang, Cavite, Philippines[2, 3, 4, 6]
Research Center, Cavite State University, Indang, Cavite, Philippines[5]
Research and Extension, Cavite State University – CCAT, Rosario, Cavite, Philippines[7]

***Abstract*—Traditional sun drying remains the primary practice among smallholder coffee farmers in the Philippines, often leading to an inefficient and inconsistent drying process. While transitioning to mechanical drying improves product quality, achieving uniform airflow in cabinets with multiple trays often requires costly post-fabrication modifications, resource-intensive trials, and repetitive field testing to fine tune the performance of the system. To reduce inefficient and repetitive trial-and-error procedures, a pre-fabrication design verification of a small-scale mechanical cabinet dryer was conducted using COMSOL Multiphysics. This study explores how the dryer's geometry influences its aerodynamic and thermal performance under baseline, no-load conditions prior to fabrication. The system was simulated to deliver an inlet air velocity of 1.56 m/s and a controlled heat flux to maintain 40°C. Results revealed steady pressure equalization within the plenum chamber, which successfully mitigated non-uniform airflow. As a result, a relatively high Velocity Uniformity Index of 0.84 was achieved across the tray layers. In addition, internal turbulent mixing contributed to a more stable thermal profile, reaching a near-ideal Temperature Uniformity Index of 0.99. These findings reveal that the core geometry of the dryer performs well from an aerodynamic standpoint. By achieving flow equalization in a no-load setting, the study provides an optimized baseline design, helping reduce the need for extensive trial-and-error during future prototyping and testing under actual operating conditions.**

***Keywords*—COMSOL Multiphysics; coffee dryer; heat transfer; design verification; aerothermal simulation; performance characterization**

I. Introduction

Drying is considered the most common and oldest technique for preserving agricultural crops, where moisture content and water activity are reduced to minimize chemical, biochemical, and microbiological deterioration [1][2][3]. This postharvest process is recognized as the most critical step affecting the final quality of the coffee [4][5][6][7]. Apart from influencing the physical appearance of the coffee beans, drying can also influence the quality of the end-product of the hulling process [5][8].

Open sun drying is still widely used nowadays for drying agricultural products even in various developing countries with the goal of lowering the moisture content of the beans [9][10][11]. However, this traditional approach poses several risks including contamination, longer drying period and unpredictable weather patterns and conditions [11]. Despite its low cost and simplicity that attracts coffee growers [11], sun drying approach is not recommended due to numerous factors that could threaten the quality of the product [10].

Sun drying, as a weather-dependent process, could take up two to three weeks which makes it a slow process that requires regular stirring to ensure even drying [11]. Drying coffee on open pavements usually takes several days, depending on the type of processing. Washed coffee generally dries in about six to seven days, pulped natural or semi-washed coffee needs roughly eight to nine days, and natural or dry-processed coffee requires the longest, often around 12 to 14 days [12]. Apart from that, the harvesting season for coffee coincides with the rainy season of the year. This makes the process labor-intensive, as the commodity should be covered during adverse weather conditions [11]. Furthermore, extended drying periods increase the likelihood of microorganisms, molds, and mycotoxins developing, which can compromise the quality of the product [10]. This includes contamination by dust, insects, and other domestic animals. All these factors prevent the coffee farmers from utilizing alternative, and more efficient drying methods when traditional sun drying is not possible [12].

Aside from traditional open sun drying, some common methods for drying the coffee cherries are the solar and mechanical drying [10][13][14][15]. The use of solar energy in drying later expanded to include solar dryers. These systems improve drying efficiency and help reduce problems such as mold growth and microbial contamination. However, because they rely entirely on sunlight, unstable weather can still hinder their performance. In coffee processing, solar drying offers an advantage: temperatures generally stay below 50°C, which preserves the embryo inside the bean. Once this temperature is exceeded, the embryo can be damaged, leading to rapid internal deterioration and lower overall quality [10][16]. On the other hand, mechanical drying serves to accelerate the slowest segment of the drying curve, specifically the drop from 15% to 11% moisture, thereby minimizing the risk of unnecessary fermentation [12]. Moreover, mechanical dryers were found to preserve significantly higher levels of phenolic compounds and antioxidant activity compared to sun drying [17]. Through the use of a mechanical dryer, water activity was maintained below 0.6 and with a stable moisture content of 7.7–10.4%, conditions that effectively inhibit microbial growth and prevent mycotoxin formation [18].

These advantages, however, are highly dependent on the internal geometry of the cabinet and its capacity to deliver uniform airflow and stable temperatures across all tray levels. Non-uniform drying in such dryers is primarily caused by poor airflow distribution through the chamber, which can be improved by optimizing the flow path and ensuring more uniform velocity across trays [19]. Repetitive field testing through trial-and-error is costly and time-consuming, making simulation a practical alternative for evaluating dryer performance before physical prototypes are developed.

This study computationally characterizes the aerodynamic and thermal performance of a small-scale mechanical coffee cabinet dryer using COMSOL Multiphysics under steady-state, no-load conditions. Isolating the pressure and velocity distributions across the plenum and intermediate ducts enables a direct evaluation of the system's capacity to achieve foundational flow equalization. Verifying that the core geometry performs well from an aerodynamic standpoint validates the underlying structural design, helping reduce the need for extensive trial-and-error during future physical prototyping and testing under actual operating conditions.

II. Literature Review

Before the physical fabrication, computational simulation enables a controlled environment to study and analyze airflow behavior, heat distribution, and other key performance parameters while minimizing uncertainties in the design process. Understanding and optimizing these dynamics is crucial for producing high-quality output, extending shelf life, and supporting broader goals of food safety and sustainability [17]. This goal can be achieved through proper modelling of heat and airflow dynamics across the system [20].

In recent years, Computational Fluid Dynamics (CFD) has been recognized as a critical tool for diagnosing and correcting non-uniform airflow, which is the primary cause of uneven drying in cabinet systems, and recent literature strengthens its role in dryer optimization. Advancements in CFD modeling have shifted attention toward achieving uniform velocity distribution, with iterative design refinements based on simulation outputs becoming standard practice for improving dryer performance [21]. Flow stratification and non-uniform drying are well-documented drawbacks of cabinet drying systems. However, optimizing internal geometry through the precise modeling of heat and airflow dynamics can significantly mitigate these issues. Existing studies show that optimizing cabinet geometry and airflow pathways not only enhances uniformity but can generate substantial efficiency gains, including up to a 50 percent reduction in drying time and overall energy use, especially when combined with heat pump technology [19][21][22][23][24][25]. Furthermore, the reliability of this computational approach is confirmed by experimental validations, which consistently demonstrate less than a 10 percent relative error between simulated and physical values when predicting complex airflow behaviors and recirculation zones.

For instance, a CFD-integrated sequential linear programming framework was utilized to systematically evaluate the influence of supply fan positions on airflow uniformity in a multi-tray cabinet dryer [22]. The study achieved a highly uniform airflow range of 0.82–1.9 m/s, underscoring the effectiveness of CFD-based geometric optimization. However, it was emphasized that the absence of thermal coupling and experimental validation in purely aerodynamic simulations is a crucial limitation since temperature variations may become the next limiting factor. Therefore, comprehensive optimization frameworks must integrate both aerodynamic and thermal uniformity.

To establish a reliable aerothermal baseline before introducing the complex variables of agricultural products, several studies evaluated drying systems under no-load, steady-state conditions. A generalized methodology for the thermal testing of cabinet and solar dryers in no-load conditions has been developed, utilizing a no-load performance index (NLPI) to accurately compare structural designs [25]. Building on this principle, explicitly evaluating the temperature and air-velocity distribution inside an empty drying chamber has been demonstrated as a necessary prerequisite to verify a system's thermal and aerodynamic behavior before loading the product [24]. Furthermore, computational tools such as COMSOL Multiphysics have been successfully utilized for the finite-element modeling of dryers under no-load conditions, with simulated thermal data validated against physical experimental tests [23]. Overall, these insights reveal that CFD functions both as a diagnostic framework and a design optimization tool, enabling evidence-based improvements in drying uniformity, system efficiency, and the overall performance of cabinet dryers.

III. Materials and Methods

A. Computational Domain and Dryer Geometry

The coffee cabinet dryer was developed using Autodesk Fusion 360 computer-aided design (CAD) software. The 3D computational domain encompasses the internal fluid volume of the system's major assemblies: the plenum chamber, air routing duct, and the double-walled, fiberglass-insulated drying chamber containing a 5-layer stainless-steel tray assembly (Fig. 1).

Fig. 1. Full 3D CAD model of the proposed mechanical coffee cabinet dryer.

To establish a reliable baseline before introducing the complex variables of agricultural products, the internal domain was modeled under no-load conditions. The tray levels were treated as unobstructed fluid volumes, isolating the aerodynamic performance of the structural geometry to ensure that any observed flow stratification is a direct result of the cabinet's

architecture rather than the variable hydraulic resistance introduced by coffee beans (Fig. 2).

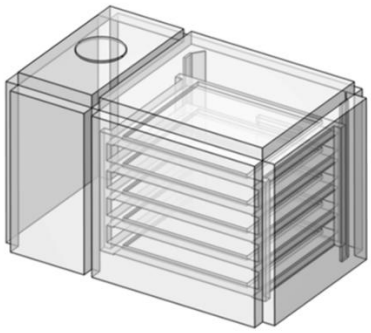

Fig. 2. Extracted computational domain representing the internal fluid volume for CFD analysis.

B. Design Assumptions and Governing Equations

The numerical simulation was executed in COMSOL Multiphysics based on several simplifying physical assumptions to ensure computational efficiency while maintaining acceptable aerothermal accuracy:

1) Incompressible flow: Airflow operates at low Mach numbers; therefore, density variations are negligible, and the fluid is treated as incompressible.

2) No internal heat generation: Heating originates externally from the simulated heating element; there is no volumetric heat generation within the drying chamber itself (Q = 0).

3) Adiabatic boundaries: Because the physical prototype utilizes thick fiberglass lagging, the external walls are treated as perfectly insulated.

The physical phenomena inside the dryer were governed by the conservation of mass, momentum, and energy. Mass conservation for the incompressible fluid is defined by the continuity equation:

$$\nabla \cdot u = 0 \tag{1}$$

Because the forced convection driven by the supply fan induces high-velocity gradients and internal recirculation, the airflow was characterized as turbulent. Momentum transport was resolved using the Reynolds-Averaged Navier-Stokes (RANS) formulation:

$$\rho\left(\frac{\partial t}{\partial u} + u \cdot \nabla u\right) = -\nabla p + \nabla \cdot [(\mu + \mu t)(\nabla u + (\nabla u)T)] \tag{2}$$

Turbulence effects were modeled using the Realizable k–ε model, which provides robust predictions for internal flows with rotational features and flow separation. The turbulent eddy viscosity (μ_t) is defined as:

$$\mu t = C\mu\frac{k^2}{\varepsilon} \tag{3}$$

To fully describe the thermal behavior inside the dryer, the general convection-conduction energy balance was applied to couple the thermal distribution with the velocity field:

$$\rho C p u \cdot \nabla T + \nabla \cdot q = Q + Qp + Qvd \tag{4}$$

where, $\rho C_p u \cdot \nabla T$ represents the dominant convective heat transport by the airflow, and $\nabla \cdot q$ models the conductive heat transfer through the solid boundaries of the system. The parameter Q corresponds to the external volumetric heat source, whereas Q_p represents the work associated with pressure changes, and Q_{vd} accounts for heating due to viscous dissipation.

Under the low Mach number and low-velocity operating conditions considered in this study, the effects of pressure work (Q_p) and viscous shear heating (Q_{vd}) are negligibly small. Consequently, these terms are systematically treated as zero within the numerical solver.

C. Boundary Conditions and Thermal Control Logic

The simulation boundary conditions were established to precisely replicate the intended operational parameters of the physical prototype. Aerodynamically, a velocity inlet boundary condition of 1.56 m/s was applied at the air duct entry, corresponding to a steady volumetric flow rate of 0.03 m³/s. The exhaust vent at the top of the cabinet was modeled as a pressure outlet set to standard atmospheric pressure, expressed as 0 Pa gauge pressure, permitting the free discharge of the circulating air into the ambient surroundings. All internal structural walls, baffles, and tray supports were assigned a standard no-slip condition (u = 0).

To establish the internal thermal environment, a fixed air temperature boundary condition of 373.15 K (100°C) was imposed at the outlet of the heating plenum chamber, immediately upstream of the connecting air duct leading into the drying chamber. This represents the temperature of the conditioned process air supplied by the heating system prior to distribution within the cabinet. Because the physical cabinet utilizes thick fiberglass lagging, the external boundaries were approximated as adiabatic to isolate the internal thermal distribution. However, to account for minor structural conductive losses and accurately model the target internal drying environment of 313.15 K (40°C), a constant surface heat flux of 180 W/m² was applied to the external walls.

Furthermore, to evaluate the transient thermal response of the system under operational conditions, the heating element was governed by an ON/OFF thermostat rule with hysteresis. This control logic dynamically regulated the average domain temperature (T_{avg}) by defining the volumetric heat source density, $q''(t)$ in W/m³, based on predefined lower (T_{on}) and upper (T_{off}) temperature thresholds. The governing control logic for the heat source is mathematically expressed as a piecewise function:

$$q''(t) = \begin{cases} q_0 & if\ T_{avg} \leq T_{on} \\ 0 & if\ T_{avg} \geq T_{off} \\ Interpolated & if\ T_{on} < T_{avg} < T_{off} \end{cases} \tag{5}$$

where, T_{on} is the lower temperature threshold, T_{off} is the upper temperature threshold, and q_0 is the maximum heat source capacity. This hysteresis formulation ensures realistic thermal cycling, preventing high-frequency artificial oscillation in the

numerical solver while accurately reflecting the thermal buffer capacity of the physical drying chamber.

D. Mesh Generation and Grid Independence

The resolution of the computational model, determined by the mesh parameters, governs how the Finite Element Method breaks down the drying chamber geometry into simple elements. Achieving greater accuracy requires a finer mesh, but this refinement directly increases both the necessary computation time and memory resources [20]. The simulation pipeline used in this study was adapted from the study of [20], which involves the CFD model analysis of a multipurpose dryer (Fig. 3).

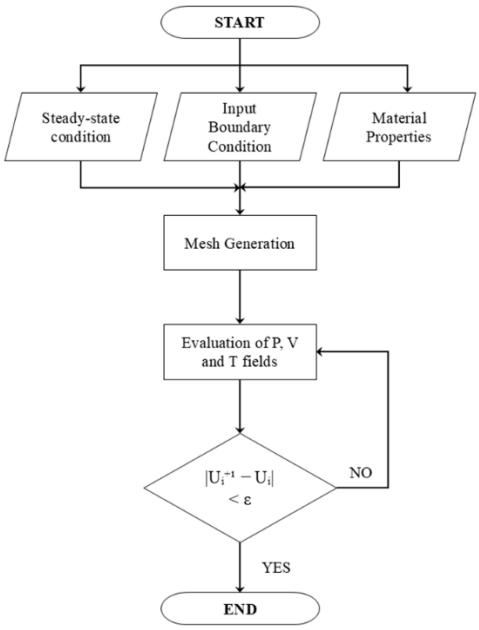

Fig. 3. Adapted simulation pipeline based on the framework presented in [20].

With the governing physics and operational boundaries fully defined, the computational domain required spatial discretization to resolve the flow and temperature fields. A physics-controlled, unstructured mesh utilizing 3D tetrahedral domain elements and triangular boundary elements was generated across the three primary domains elaborated in Table I.

TABLE I. MESH STATISTICS FOR THE THREE MAJOR DOMAINS

Computational Component	Domain Elements (Tetrahedra)	Boundary Elements (Triangles)	Edge Elements (Edges)	Total Elements
Drying Chamber	417,186	46,268	3,114	466,599
Plenum Chamber	27,492	7,642	800	35,394
Air Duct	70,820	9,920	680	81,420

To guarantee that the predicted aerothermal fields were independent of discretization error, a grid independence study was performed. Four progressively refined meshes were evaluated, consisting of approximately 495,566; 527,053; 606,877; and 749,110 total elements (Fig. 4).

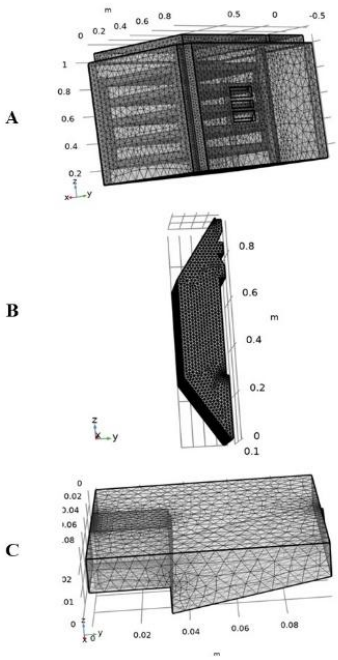

Fig. 4. Generated mesh for each computational domain: (A) Drying chamber; (B) Air duct; and (C) Plenum chamber.

The placement of virtual sensors was strategically designed to capture the full gradient of the aerothermal environment. Specifically, point probes were positioned on all interior boundary surfaces of the drying chamber's domain to monitor wall-proximate effects. Furthermore, probes were localized at the geometric center of each of the tray layers, ensuring that the refinement analysis accounted for the critical airflow and temperature variations within the product-loading zones.

To assess convergence across these iterations, six sensitive virtual probe locations were defined within the computational domain including the heated air inlet, the front and center of the third tray, and representative chamber walls to systematically monitor temperature variations across each successive refinement.

E. Simulation Strategy

The investigation was divided into two distinct computational phases. A steady-state simulation characterized the baseline aerodynamic behavior of the system, with emphasis on airflow distribution, static pressure equalization, and overall flow uniformity. A subsequent transient simulation spanning 60 minutes evaluated the system's thermal response and the performance of the thermostat control logic.

The segregated solver employed pseudo-time stepping with Anderson acceleration, successfully achieving stable convergence for both fluid flow and turbulence variables. To capture the transient thermal response during this 60-minute evaluation, point probes were strategically positioned at the system inlet, the exhaust outlet, and along the edge of each tray layer farthest from the air inlet. This conservative placement ensured that the most critical, time-dependent heating curves were accurately monitored.

F. Data Extraction and Evaluation Metrics

To objectively quantify flow equalization and thermal homogeneity, horizontal evaluation planes were established at each tray level. Data extraction was performed across these planes, and the system's performance was evaluated using two dimensionless indices.

The Velocity Uniformity Index (VUI) and Temperature Uniformity Index (TUI) were calculated based on the area-weighted relative standard deviation of the flow fields:

$$\text{VUI} = 1 - \frac{\sigma_v}{\bar{v}} \quad (6)$$

$$TUI = 1 - \frac{\sigma_T}{\bar{T}} \quad (7)$$

where, σ_v and σ_T are the standard deviations of velocity and temperature across the respective evaluation planes, and $\bar{v}$ and $\bar{T}$ represent the corresponding area-weighted mean velocity and temperature. Values approaching 1.0 indicate optimal uniformity across the evaluated plane.

In addition to planar data, discrete monitoring points were utilized for localized analysis. Point probes were strategically placed at the center of the front face of each of the five tray layers. These probes were positioned at the furthest extremity from the air duct inlet to capture the potential "dead zones" or areas of maximum thermal lag, providing a conservative estimate of the drying conditions at the most critical locations within the chamber.

IV. Results

A. Scope and Limitations of the Simulation Study

A full-scale three-dimensional model of the coffee cabinet dryer was analyzed based on its actual geometric dimensions and intended operating parameters. The present investigation is strictly limited to simulation-based performance characterization under no-load conditions.

Since this is a foundational pre-fabrication analysis, key operational metrics heavily dependent on agricultural variables such as drying rate, moisture removal efficiency, specific energy consumption, and final product quality were not experimentally validated. Moreover, this study emphasizes aerothermal performance assessment through validated numerical modeling, establishing the necessary aerodynamic baseline required before future experimental validation and full-load drying kinetics can be quantified.

B. Simulation Performance and Convergence

The segregated solver, employing pseudo-time stepping together with Anderson acceleration, provided stable convergence for the coupled velocity, pressure, turbulence, and heat transfer equations. Convergence for the steady-state domains was achieved within approximately 130 to 170 iterations, with residuals reduced to acceptable tolerances for both fluid flow and turbulence variables. Similar convergence behavior was observed in the plenum and drying chamber simulations. This confirms that the numerical model was capable of predicting steady-state airflow and heat transfer characteristics within the dryer configuration.

The solution time ranged between 20 and 25 minutes for steady-state simulations, while the transient simulations incorporating the piecewise thermostat control logic required approximately 7 to 8 minutes. The convergence profile validates the robustness of the numerical model and supports its suitability for evaluating the aerothermal design of the cabinet prior to physical fabrication.

C. Grid Independence Verification

Across successive mesh refinements, temperature variations remained negligible. The maximum observed deviation between adjacent mesh levels did not exceed 0.09°C, with relative differences remaining below 0.25% of the nominal 40°C (313.15 K) operating temperature. Notably, the heated air inlet temperature remained constant at 40°C across all mesh levels, indicating stable boundary condition implementation.

TABLE II. Grid Independence Results for Predicted Temperature Across All Probes

Mesh Level	Probe A	Probe B	Probe C	Probe D	Probe E	Probe F
h1.0	40.00	39.95	39.93	39.94	39.94	39.94
h1.5	40.00	39.95	39.93	39.95	39.95	39.94
h2.0	40.00	39.95	39.94	39.96	39.95	39.95
h2.5	40.00	39.93	39.90	39.94	39.93	39.92
% Error	**0.00%**	**0.06%**	**0.09%**	**0.05%**	**0.06%**	**0.07%**

As presented in Table II, the temperature values across all six monitoring locations exhibited high stability as the mesh density increased. The primary boundary condition at the inlet (Probe A) remained constant at 40.00°C, confirming that the refinement process did not introduce numerical instabilities at the source. For the internal regions, particularly at the front and center of the third tray (Probes B and F), the temperature variations between successive refinements were minimal, settling at approximately 39.93°C to 39.95°C. The convergence was quantitatively assessed using the relative error between the medium-fine (h2.0) and extremely fine (h2.5) mesh levels. The results indicated that the maximum relative error did not exceed 0.09%, occurring at probe C. In the central drying zones, the error remained below 0.07%.

Based on the numerical stability observed across the mesh iterations, the configuration consisting of 606,877 elements (h2.0) was determined to provide sufficient spatial resolution. The transition to the finest mesh (749,110 elements) yielded a maximum relative error of less than 0.09%, indicating that further refinement offered negligible improvements in precision. Consequently, the h2.0 mesh was selected for all subsequent steady-state and transient simulations to optimize the balance between numerical accuracy and computational efficiency.

Furthermore, no monotonic drift in predicted values was observed with increasing mesh density. Therefore, the mesh containing 606,877 elements was selected as the optimal configuration, effectively balancing computational efficiency and numerical accuracy. This grid independence validation confirms that the velocity, pressure, and temperature fields presented in subsequent sections are strictly mesh-independent and physically reliable.

D. Aerodynamic Performance and Flow Distribution

Achieving a uniform velocity profile across all tray levels is the primary fluid dynamic challenge in multi-tray batch dryers, as non-uniform flow directly induces heterogeneous moisture content [21].

1) Airflow path, velocity uniformity, and intermediate duct dynamics: The inlet boundary condition was set to a velocity of 1.56 m/s at the air duct entry, corresponding to a volumetric flow rate of 0.03 m³/s. The velocity contours (Fig. 5) confirm a peak magnitude of 1.51 m/s within the duct, validating the boundary setup. The high-momentum air builds up in the large plenum chamber, where heating and initial pressurization occur. The conditioned air then exits the plenum and passes through an intermediate air duct before entering the main drying chamber, a configuration intended to redistribute flow pressure and ensure delivery to the base of the tray stack. Within this intermediate duct, the flow velocity is observed to increase due to the reduced cross-sectional area, creating a highly directional jet entering the drying volume.

Within the main drying zone (the volume encompassing the six trays), the air velocity streamlines (Fig. 6) display a highly desirable parallel flow regime as the flow expands and passes through the trays. The velocity magnitude over the virtual coffee bed volume consistently falls within the range of 0.5 m/s to 1.0 m/s. This narrow range indicates a high degree of flow uniformity.

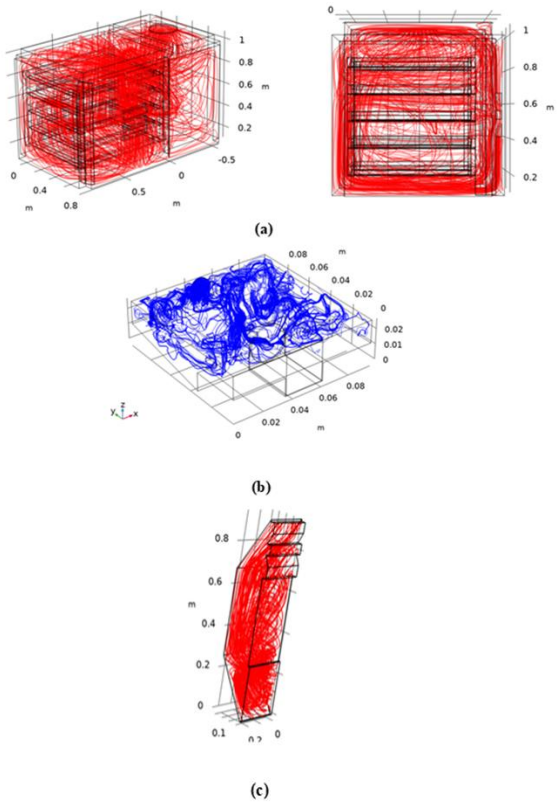

Fig. 5. Streamline visualization of the velocity field in different computational domains: (a) Drying chamber; (b) Air duct; and (c) Plenum chamber.

Assuming an approximate characteristic length (hydraulic diameter) corresponding to the tray spacing, the Reynolds number (Re) calculated for the flow through the drying zone suggests a regime transitioning from laminar to mildly turbulent. This condition is advantageous, as it provides sufficient convective heat transfer without incurring excessive fan power consumption or risk of entraining lighter particles. The minimal localized recirculation zones observed in the far corners of the plenum are low-energy eddies that rapidly decay. The flow entering the intermediate duct is stable, confirming that the initial air distribution within the plenum is effective.

2) Quantitative velocity uniformity assessment: To quantitatively evaluate airflow distribution, the Velocity Uniformity Index (VUI) was computed for each tray surface. The Velocity Uniformity Index (VUI) quantitatively evaluated airflow distribution across the multi-tray system, yielding a global value of 0.84 that indicates highly effective overall balance (Table III).

TABLE III. VELOCITY UNIFORMITY INDEX INSIDE THE DRYING CHAMBER

Location	Individual VUI	Global VUI
Tray No. 1	0.76	0.84
Tray No. 2	0.88	
Tray No. 3	0.87	
Tray No. 4	0.86	
Tray No. 5	0.86	

While Tray 1 showed a modestly lower VUI of 0.76 due to localized jet effects from its proximity to the intermediate duct discharge, upper trays achieved superior uniformity of 0.86 – 0.88 through progressive plenum-driven redistribution, outperforming baseline CFD-optimized designs reporting 0.766–0.80 VUI found in several studies [22][26]. Furthermore, velocities across all evaluation planes remained above stagnation thresholds (>0.5–1.0 m/s), eliminating dead zones and confirming the system's efficacy relative to plenum-enhanced prototypes achieving similar flow homogenization.

Nevertheless, to further improve the aerodynamic uniformity at the lowest tray level prior to physical fabrication, a geometric flow-conditioning modification is proposed at the intermediate duct discharge region. Specifically, integrating a passive flow-correcting element, such as an angled deflector wedge or perforated distribution baffle plate, would mechanically disrupt and diffuse the concentrated high-momentum jet before it impinges on Tray 1. This modification is expected to promote earlier lateral airflow redistribution within the lower plenum region, thereby reducing localized velocity gradients and increasing the Tray 1 VUI toward the more balanced profiles observed in the upper trays.

3) Pressure distribution, hydraulic resistance, and flow equalization: The pressure field (Fig. 7) is perhaps the most compelling result validating the dryer's aerodynamic function. A substantial static pressure peak, exceeding 30 Pa, is successfully established in the plenum immediately adjacent to the air inlet. This pressure acts as the necessary reservoir to

overcome the cumulative hydraulic resistance of the intermediate duct and the subsequent six stacked trays and the coffee product, which will be modeled as a porous medium in subsequent studies.

The principle of flow equalization in multi-tray systems dictates that the pressure drop across the product ($\Delta P_{product}$) must be significantly larger than the velocity pressure variations within the plenum (ΔP_{plenum}) to ensure a consistent flow rate ($\dot{m}$) through each layer. The highly uniform static pressure profile observed beneath the lowest tray suggests that ΔP_{plenum} is negligible compared to the expected $\Delta P_{product}$. The smooth, progressive decrease in pressure moving vertically through the drying chamber, terminating near ambient (zero-gauge) pressure at the exhaust, confirms that the static pressure gradient successfully drives the air across the entire volume. This robust pressure differential fundamentally mitigates the stratification and non-uniform drying characteristic of passively vented systems [20].

E. Thermal Homogeneity

Thermal homogeneity is essential for product quality, particularly for coffee, where temperature excursions above 50°C can initiate irreversible physicochemical damage, compromising final cup quality [16].

1) Thermal mixing and energy balance within the plenum: The simulation employed a high heater outlet temperature of 100°C (373.15 K) as the boundary condition. The temperature gradient reveals a remarkable degree of thermal dissipation within the plenum volume (Fig. 8). The high-velocity, high-temperature air jet interacts immediately with the large, relatively quiescent volume of the plenum. This promotes intense turbulent mixing, causing the air temperature to rapidly reduce and settle into a narrow operational range of 41°C to 45°C (314 K to 318 K) as it enters the intermediate duct.

This rapid stabilization which results in a narrow ±4 K deviation around the target 40°C (313.15 K) confirms effective heat balance. The internal metallic walls and tray structure act as a thermal buffer and heat sink, ensuring thermal energy is distributed uniformly across the plenum's cross-section. The applied external surface heat flux of 180 W/m² successfully counteracts minor conductive losses, preserving the near-adiabatic state of the system. By confirming that the drying air is uniformly applied at a moderate temperature, the simulation provides confidence that the mechanical dryer will preserve the cellular structure, color, and subsequent sensory profile of the coffee.

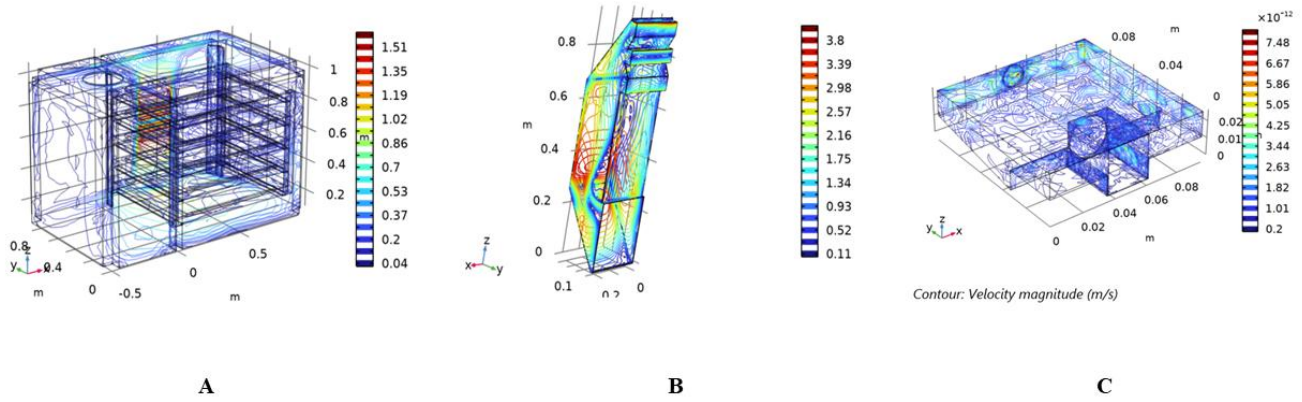

Fig. 6. Contour visualization of the velocity magnitude (m/s): (A) Drying chamber; (B) Air duct; and (C) Plenum chamber.

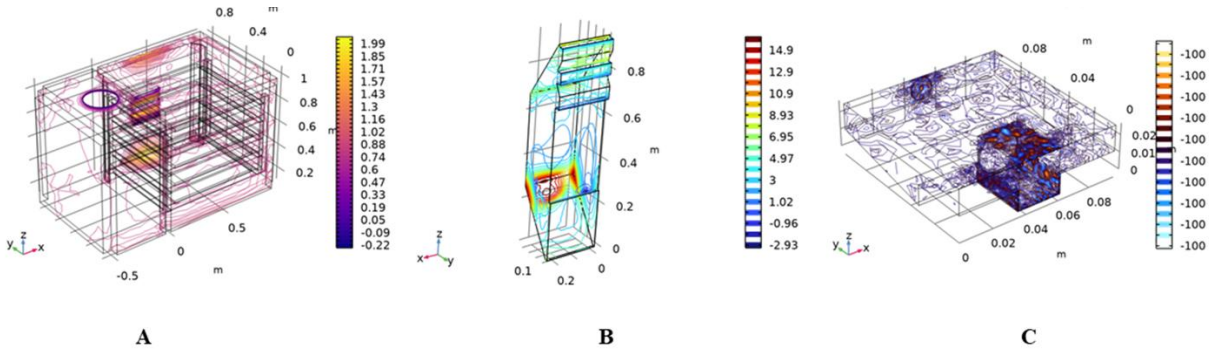

Fig. 7. Contour visualization of the Pressure in Different Domains: (A) Drying chamber; (B) Air duct; and (C) Plenum chamber.

2) Quantitative thermal uniformity assessment: Resulting Temperature Uniformity Index (TUI) demonstrates exceptionally high thermal homogeneity, with a global TUI of 0.99 and individual tray values of 1.00.

While these values approach spatial homogeneity and may appear unusually ideal, they represent the physically coherent thermal behavior of the system under controlled, no-load conditions. The absence of a porous coffee bed eliminates spatially varying permeability and evaporative cooling effects. Under steady-state forced convection with insulated boundaries and intensive plenum mixing, the energy equation naturally converges toward a smooth temperature field without numerical artifacts (Table IV).

TABLE IV. TEMPERATURE UNIFORMITY INDEX INSIDE THE DRYING CHAMBER

Location	Individual TUI	Global TUI
Tray No. 1	1.00	0.99
Tray No. 2	1.00	
Tray No. 3	1.00	
Tray No. 4	1.00	
Tray No. 5	1.00	

This inherent tendency toward thermal equilibration is further reinforced by the aerodynamic configuration of the plenum chamber. Because the heating element is located within a relatively large plenum volume, the incoming high-temperature jet undergoes substantial turbulent mixing before entering the tray stack. The interaction between the hot inlet stream and the plenum walls promotes rapid dissipation of localized thermal gradients and facilitates cross-sectional energy redistribution. Consequently, by the time the airflow reaches the intermediate duct and drying chamber, it has already achieved significant thermal stabilization, thereby limiting the potential for downstream stratification.

The pressure distribution within the system complements this thermal behavior. The establishment of a stable static pressure reservoir in the plenum ensures nearly uniform mass flow across all tray levels. When airflow is evenly distributed and tray geometries are identical, convective heat transfer coefficients remain spatially consistent. This balanced mass flow minimizes localized overheating or underheating, directly supporting the high uniformity reflected in the TUI values. Furthermore, the chamber walls were modeled as thermally insulated, approximating near-adiabatic operation. By limiting asymmetric external heat losses, the model suppresses lateral temperature gradients that could otherwise arise from environmental interactions. The combined effect of insulated boundaries, balanced mass flow, and intensive plenum mixing creates conditions under which temperature deviations are inherently minimal.

Overall, the near-unity TUI values do not indicate numerical artifact or over-idealization; rather, they represent the physically coherent thermal behavior of the system under controlled, no-load conditions. It is expected that the incorporation of porous media modeling and coupled moisture transport in future full-load simulations will introduce additional spatial variability due to evaporative cooling and heterogeneous resistance effects, thereby yielding more conservative yet operationally representative uniformity indices.

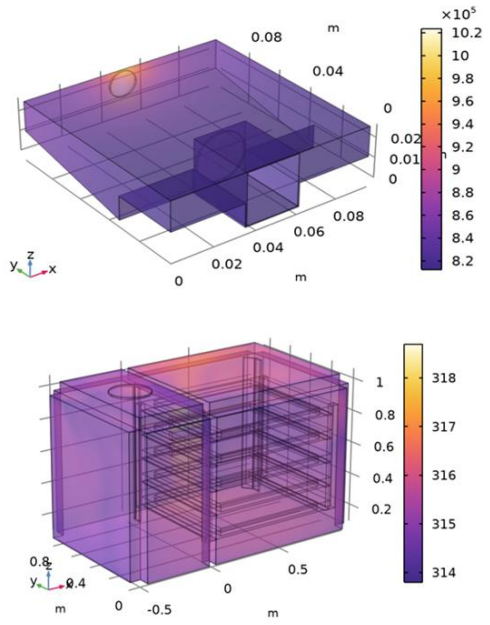

Fig. 8. Temperature distribution within the modeled volume.

F. Transient Thermal Response

In addition to steady-state mapping, a time-dependent simulation was conducted over a 60-minute period. Temperature evolution was monitored using point probes strategically placed at the system inlet, outlet, and along the side of each tray farthest from the air inlet to represent a conservative case for heat delivery. The temporal profiles indicate a rapid rise in air temperature during the initial heating phase, followed by a gradual approach toward steady-state conditions. The inlet and outlet temperature histories show that the system stabilizes within the target operating range after the initial transient period, with minimal temperature divergence observed between the inlet and outlet once equilibrium is reached. This behavior suggests effective thermal regulation and supports the assumption of near-adiabatic operation (Fig. 9).

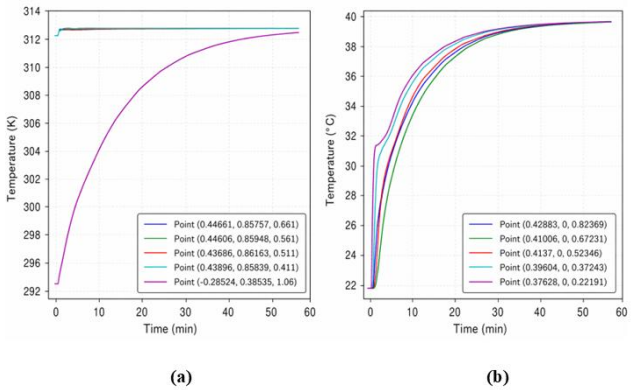

Fig. 9. Transient temperature profiles of the mechanical coffee cabinet dryer obtained from a 60-minute time-dependent CFD simulation. (a) Temperature evolution at selected points near the air inlet and outlet, showing rapid initial heating followed by stability.

Furthermore, the tray-level responses exhibit consistent heating trends across all layers. While minor differences in heating rates are observed during the early stages, all tray locations converge toward a narrow temperature band as time progresses, reaching the desired drying range even at the farthest probe locations.

V. Limitations of the Study

Despite its foundational contributions to the aerothermal design of the cabinet dryer, this study acknowledges several inherent limitations that must be addressed in subsequent research phases. Primarily, the current computational model operates strictly under no-load conditions. The absence of a physical coffee bed means that the complex aerodynamic resistance, spatially varying permeability, and localized flow channeling introduced by agricultural materials are not captured in the current velocity fields. Furthermore, the thermal evaluation is restricted to single-phase sensible heat transfer. In actual operational states, the desorption of moisture from the coffee beans will introduce multiphase mass transfer and significant evaporative cooling effects. These endothermic reactions will inherently induce localized temperature gradients, meaning the near-unity Temperature Uniformity Index (TUI) observed in this baseline study represents an idealized maximum rather than a field-loaded absolute.

VI. Conclusion

The study focused on establishing the aerothermal baseline for the proposed mechanical coffee cabinet dryer through rigorous three-dimensional computational fluid dynamics (CFD) modeling. The results demonstrated that coupling a high-pressure plenum with strategic internal routing has the capability to achieve the flow equalization and thermal stability required for effective batch drying. The aerodynamic evaluation of this architecture revealed a highly stable, parallel flow regime across the drying chamber, evidenced by a global Velocity Uniformity Index (VUI) of 0.84. Airflow velocities were maintained within the target convective range of 0.5 m/s to 1.0 m/s across all product planes, reducing the likelihood of stagnant recirculation zones. Concurrently, the thermal analysis indicated that intensive turbulent mixing within the primary plenum facilitates rapid energy dissipation and stabilization. This mechanism maintained the internal drying environment between 41°C and 45°C (314 K to 318 K), resulting in a high Temperature Uniformity Index (TUI) of 0.99 under the simulated conditions. Such thermal uniformity may help mitigate localized overheating, thereby reducing the risk of irreversible physiochemical damage to the coffee embryo and preserving final cup quality.

However, it must be explicitly emphasized that this near-unity thermal index represents an idealized baseline configuration under empty, no-load conditions. In actual drying operations, the introduction of a physical, porous coffee material will significantly alter these dynamics by introducing spatially varying hydraulic resistance, localized flow channeling, and endothermic mass transfer gradients driven by evaporative cooling. These multi-phase interactions are expected to induce localized temperature gradients, substantially lowering the uniformity indices under full-load scenarios.

Nevertheless, this pre-fabrication characterization provides simulation-based design assessment of the fluid-dynamic and thermal viability of the dryer architecture. By establishing a strictly verified computational framework, these findings secure the aerothermal baseline required for the system's physical implementation. While this study evaluated a specific small-scale dryer architecture, the CFD methodology and geometric principles of flow equalization demonstrated herein may be adapted to optimize various types of agricultural drying equipment.

Acknowledgment

This work was supported by the Cavite State University (CvSU) and the Department of Science and Technology (DOST) through the DOST-funded project titled "Technology Piloting and Commercialization of Coffee Postharvest Equipment" under the program titled "Bridging the Gap on Coffee Production and Processing through Emerging Research and Innovation for the Advancement of the Industry (CvSU BEAN Program)." The authors also express their sincere gratitude to the coffee farmers, producer organizations, Local Government Units, and partner communities across CALABARZON for their invaluable support and cooperation throughout the conduct of this work.

References

[1] A. K. Stephen and S. Emmanuel, "Improvement on the design of a cabinet grain dryer," *American Journal of Engineering and Applied Sciences*, vol. 2, no. 1, pp. 217–228, 2009, doi: 10.3844/AJEAS.2009.217.228.

[2] İ. Doymaz and M. Pala, "The thin-layer drying characteristics of corn," *Journal of Food Engineering*, vol. 60, no. 2, pp. 125–130, 2003, doi: 10.1016/S0260-8774(03)00016-0.

[3] O. Durodola, "Design and performance evaluation of a multipurpose conductive rotary dryer adapted for drying ogi," 2022. doi: 10.13140/RG.2.2.27692.33923.

[4] P. Corrêa, O. Resende, and D. Ribeiro, "Drying characteristics and kinetics of coffee berry," *Revista Brasileira de Produtos Agroindustriais*, vol. 8, no. 1, pp. 1–10, 2006.

[5] E. Menya and A. Komakech, "Investigating the effect of different loading densities on selected properties of dried coffee using a GHE dryer," *Agricultural Engineering International: CIGR Journal*, vol. 15, no. 2, pp. 231–237, 2013.

[6] P. Ghosh and N. Venkatachalapathy, "Processing and drying of coffee – a review," *International Journal of Engineering Research and Technology*, vol. 3, no. 12, pp. 784–794, 2014.

[7] B. Soeswanto, N. Wahyuni, and G. Prihandini, "The development of coffee bean drying process technology – a review," in *Proceedings of the International Conference on Agricultural Engineering and Rural Development*, 2021, doi: 10.2991/aer.k.211106.026.

[8] A. W. Aregba, P. Sebastian, and J. Nadeau, "Stationary deep-bed drying: A comparative study between a logarithmic model and a non-equilibrium model," *Journal of Food Engineering*, vol. 77, no. 1, pp. 27–40, 2006, doi: 10.1016/j.jfoodeng.2005.06.020.

[9] C. L. Oria and E. V. Palconit, "A review on possible combination of solar dryer materials for crops in the Philippines," *Engineering and Technology Journal*, vol. 7, no. 7, pp. 1328–1341, 2022.

[10] E. Duque-Dussán, J. R. Sanz-Uribe, and J. Banout, "Design and evaluation of a hybrid solar dryer for postharvesting processing of parchment coffee," *Renewable Energy*, vol. 215, p. 118961, 2023, doi: 10.1016/j.renene.2023.118961.

[11] E. M. Meja, S. K. Dubbe, A. Bekele, K. F. Wolde, and M. S. Adaramola, "Investigating the performance and optimization of solar coffee drying technologies: A systematic review," *Journal of Food Processing and Preservation*, vol. 49, no. 1, 2025, doi: 10.1111/jfpp.70028.

[12] R. G. Idago and R. S. M. Dela Cruz, *Value Chain Improvement of Robusta and Liberica Coffee*. Science City of Muñoz, Nueva Ecija, Philippines: Philippine Center for Postharvest Development and Mechanization (PhilMech), Tech. Bull., vol. 5, no. 1, 2015.

[13] A. Parra-Coronado, G. Roa-Mejía, C. E. Oliveros-Tascón, and J. R. Sanz-Uribe, *Optimización operacional de secadores mecánicos para café pergamino*. Chinchiná, Colombia: CENICAFÉ, 2017.

[14] S. Phitakwinai, S. Thepa, and W. Nilnont, "Thin-layer drying of parchment Arabica coffee by controlling temperature and relative humidity," *Food Science and Nutrition*, vol. 7, no. 9, pp. 2921–2931, 2019, doi: 10.1002/fsn3.1142.

[15] R. A. Trejos, G. Roa-Mejía, and C. E. Oliveros-Tascón, "Humedad de equilibrio y calor latente de vaporización del café pergamino y del café verde," *Revista Cenicafé*, vol. 40, no. 1, pp. 5–15, 1989.

[16] R. Osorio Hernandez, I. D. F. Ferreira Tinoco, J. Correna Carlo, J. A. Osorio Saraz, and I. D. Aristizábal Torres, "Bioclimatic analysis of three buildings for wet processing of coffee in Colombia," *Revista Facultad Nacional de Agronomía Medellín*, vol. 71, no. 3, pp. 8609–8616, 2018, doi: 10.15446/rfnam.v71n3.67772.

[17] M. B. Fauzi, E. A. Kosasih, M. I. Dzaky, G. G. Nasution, and A. Zikri, "Experimental analysis and numerical simulation of coffee bean drying in packed beds with different coffee bean stack height," *Journal of Advanced Research in Fluid Mechanics and Thermal Sciences*, vol. 128, no. 2, pp. 122–138, 2025, doi: 10.37934/arfmts.128.2.122138.

[18] D. J. M. de Abreu et al., "Influence of drying methods on the post-harvest quality of coffee: Effects on physicochemical, sensory, and microbiological composition," *Foods*, vol. 14, no. 9, p. 1463, 2025, doi: 10.3390/foods14091463.

[19] S. Misha, S. Mat, M. H. Ruslan, K. Sopian, and E. Salleh, "The prediction of drying uniformity in tray dryer system using CFD simulation," *International Journal of Machine Learning and Computing*, vol. 3, no. 5, pp. 419–423, 2013, doi: 10.7763/IJMLC.2013.V3.352.

[20] C. J. Ohagwu et al., "Computational fluid dynamic model analysis of multipurpose dryer with bio-waste heat source: An experimental validation using paddy rice," *Energy Conversion and Management X*, vol. 23, p. 100652, 2024, doi: 10.1016/j.ecmx.2024.100652.

[21] D. Cebulski and P. Cyklis, "Application of CFD simulation to the design of an innovative drying chamber," *Energies*, vol. 17, no. 13, p. 3338, 2024, doi: 10.3390/en17133338.

[22] D. A. Asrate, F. B. Tadle, and Y. D. Mihretie, "Enhancement of airflow uniformity in multi-tray dryers through a CFD-integrated sequential linear programming framework," *Scientific Reports*, vol. 16, p. 4226, 2026, doi: 10.1038/s41598-025-34360-1.

[23] L. Kumar et al., "Experimental and computational validation of thermal performance of an active greenhouse solar dryer in no-load conditions," *International Journal of Low-Carbon Technologies*, vol. 19, p. ctae036, 2024, doi: 10.1093/ijlct/ctae036.

[24] A. Jha and P. P. Tripathy, "Performance evaluation and finite element modeling of heat, mass, and fluid flow inside a hybrid solar dryer during drying of paddy grains," *Frontiers in Food Science and Technology*, vol. 4, p. 1411956, 2024, doi: 10.3389/frfst.2024.1411956.

[25] S. Singh and S. Kumar, "Testing method for thermal performance-based rating of various solar dryer designs," *Solar Energy*, vol. 86, no. 1, pp. 87–98, 2012, doi: 10.1016/j.solener.2011.09.009.

[26] M. Precoppe, S. Janjai, B. Mahayothee, et al., "Batch uniformity and energy efficiency improvements on a cabinet dryer suitable for smallholder farmers," *Journal of Food Science and Technology*, vol. 52, no. 8, pp. 4819–4829, 2015, doi: 10.1007/s13197-014-1544-y.